Hirooka *et al. Robomech J (2017) 4:25*
DOI 10.1186/s40648-017-0093-3

ROBOMECH Journal

RESEARCH ARTICLE

Open Access

# Optimization of orifice position in particle-excitation valve for proportional flow control

Daisuke Hirooka[1*], Tomomi Yamaguchi[1], Naomichi Furushiro[1], Koichi Suzumori[2] and Takefumi Kanda[3]

**Abstract**

This paper reports an improvement of the particle-excitation flow control valve. The valve that we have designed in previous reports can control air flow, using particle excitation by piezoelectric resonance, and has the following advantages: small size, lightweight, high response and continuous airflow control. However, in our previous models, the relationship between the driving voltage and the flow quantity was nonlinear. In this report, we improved the valve to realize proportional flow control. The valve consists of the orifice plate, that has some orifices, and steel particles to seal the orifices and piezoelectric transducer. It controls air flow by the voltage applied to the transducer. For proportional flow control, it is important to adjust the orifice position adequately. In this report, we optimized the orifice position, considering resonance condition of the valve. We designed the experimental prototype using a bolt-clamped Langevin type transducer and decided orifice position. And we evaluated its vibration properties and flow-rate characteristics. The experimental results showed that our designed prototype can proportionally control airflow.

**Keywords:** Proportional flow control valve, Pneumatic valve, Pneumatic actuator, PZT, Flow control valve

## Background

A pneumatic actuation system has many advantages, including lightweight, safety, and low cost. Because pneumatic actuators have compliance, they are widely researched for human support devices [1–5]. Recently, the actuators are examined as the application of artificial muscles and soft actuators [6–10]. However, it is difficult to control pneumatic equipment since air is compressible and has nonlinear characteristics. Therefore, highly controllable devices are in great demand. Many kinds of pneumatic control devices have been researched [11–28]. Especially, piezoelectric (PZT) actuators are widely used [14–22, 24–28] because some of these actuators have high response and large power. Because the strokes of PZT actuators are very small and must be increased, some researches use laminated PZTs [17–19], bimorph structure [16], motors [20, 21, 24], or displacement amplifier mechanisms [25–28]. Especially for proportional or servo valves, since the stroke of the actuated part is critical, displacement amplifier mechanisms are used. A valve with displacement amplifier mechanisms is heavy and large. We designed flow control valves using particle excitation mechanism whose advantages are small size and high response [29–32]. This control mechanism uses PZT resonance frequency and does not need the displacement amplifier mechanism. In previous report, we demonstrated its basic structure and confirmed that it has potential to provide a large flow rate [29]. We showed new mechanism of the valve using deferent types of particles for stable flow control [30]. We discussed orifice condition of the valve and designed prototype that can control air flow continuously [31]. And we expanded orifices diameter to increase flow quantity and checked responsiveness of the valve [32]. However, the flow conditions of the prototypes were nonlinear. In this report, we proposed a new model of particle-excitation valve that can realize the proportional flow control. For proportional flow control, we optimized the orifice position considering vibration mode. Firstly, we showed

*Correspondence: hirooka@kansai-u.ac.jp
[1] Department of Mechanical Engineering, Kansai University, 3-3-35, Yamate-cho, Suita-shi, Osaka 564-8680, Japan
Full list of author information is available at the end of the article

the basic mechanism and then specifically explained its design, how the valve makes the flow condition proportional. Secondly, we designed a prototype optimizing the orifice position. To decide orifice position, we used the approximation of orifice deformation shape. Next we showed the designed prototype's basic characteristics. Finally, we provided the results of a flow rate change experiment and explained the flow rate characteristics.

## Proportional mechanism using particle excitation valve

### Basic control mechanism of particle excitation

Firstly, we explain the basic principle of the previously designed particle-excitation mechanism [29]. Figure 1 shows a cross section of a flow control valve and establishes its basic working principle using particle excitation. This valve consists of an orifice plate, a piezoelectric transducer, and steel particles. The orifice plate is located at the transducer's antinode. Figure 1a depicts the valve in non-driving state. Airflow is supplied from the airport, as shown by the large arrow in Fig. 1. Particles are carried on the orifices by the supplied airflow. Since the supplied airflow presses particles onto the orifices and they work like poppets, the valve is normally closed. Figure 1b shows the valve's driving state. The small arrow shows the vibration direction. In this state, the control valve is excited by the transducer's resonance frequency. Therefore, deformation is generated at the orifice plate, and the vibration force moves the particles away from the orifice plate. As a result, air flows through the opened orifices. To control the flow rate, the vibration is changed so that the number of opened orifices is altered. Thus, the airflow can be controlled by changing the voltage applied to the transducer. In this mechanism, the moving particles could close the orifices irregularly. However, when the resonance frequency is large, the closing time becomes so short and the effect is ignorable. This working principle does not need a mechanism to locate and fix the poppets and we expect that the device can be downsized. In addition, because this valve uses the PZT transducer, the valve has potential for high response. The switching time of the valve using this mechanism was approximately 5 ms [32].

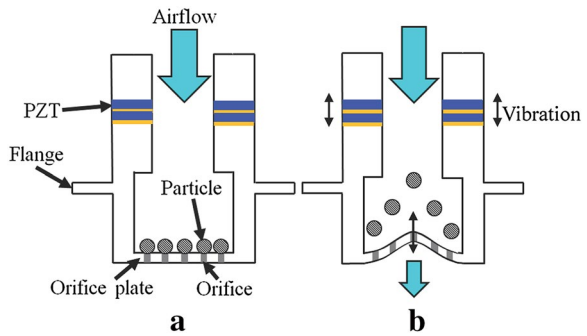


**Fig. 1** Basic control mechanism of control valve **a** non-driving state, **b** driving state

The orifice opening condition is determined by the balance between the pneumatic force and the particle's vibrational force [29]. The pneumatic force is decided by:

$$F_1 = \pi r^2 P \pm mg, \tag{1}$$

where $F_1$ is the force pressing the particle onto the orifice, $P$ is the supplied air pressure, $r$ is the orifice radius, $m$ is the particle mass, and $g$ is the gravity acceleration. The maximum particle's vibration force is:

$$F_2 = -A\omega^2 m \sin \omega t, \tag{2}$$

where $F_2$ is the vibration force, $A$ is the amplitude of the particles, and $\omega$ is the angular frequency when driving voltage frequency $f$ is defined as $\omega = 2\pi f$. If $F_2$ is larger than $F_1$, the particles move away from the orifices.

Using Eqs. (1) and (2), the orifice opening condition is calculated:

$$a > \frac{\pi r^2 P \pm mg}{m}, \tag{3}$$

where $a$ means the particle's acceleration and $a$ is defined as $a = A\omega^2$.

When using the resonance vibration, the frequency is constant. Therefore, from Eq. (2), $F_2$ is dependent on $A$, which has the same orifice plate displacement value when the particle is on orifice. The orifice plate displacement is controlled by changing the voltage applied to the transducer. In previous reports, for continuous flow control, we arranged orifices from the center at 0.2-mm intervals [31, 32]. However, in that mechanism, orifice plate deformation condition was not considered and flow condition was nonlinear. In this report, we designed a prototype in which the orifice position is optimized with consideration of the orifice deformation condition for proportional control.

We used 0.8 mm diameter particles of stainless steel (density: $7.93 \times 10^3$ kg/m$^3$), and each particle mass was 2.13 mg. When the $P$ parameter is 0.4 MPa and $r$ parameter is 0.2 mm, $a$ parameter is 23.6 km/s$^2$. This value is larger than gravity acceleration and gravity effect is ignored when each particle is on orifice.

### Proportional condition

This section explains the proportional air flow control method. Figure 2 shows the aspects of the flow rate change and the vibration displacement of the orifice plate. Figure 2a is a cross section of the orifice plate and the particles. The orifice plate has four same scale orifices as examples, located at different distances from its center. When the

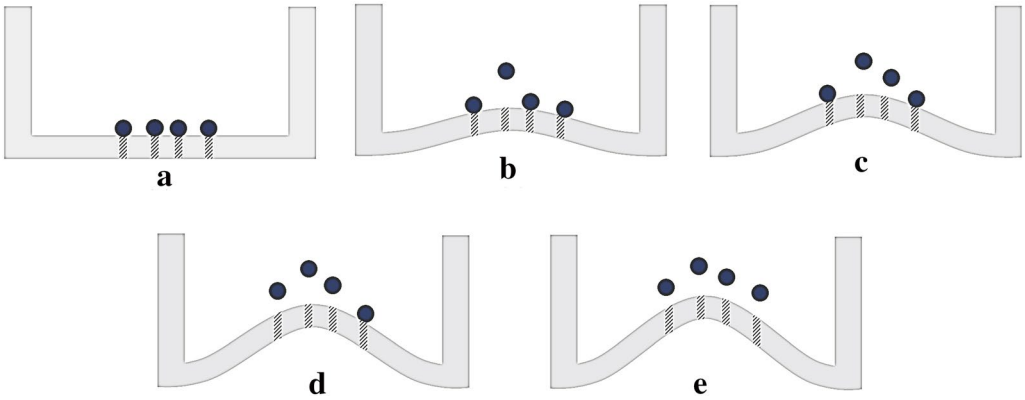


**Fig. 2** Aspects of flow rate change and vibration (**a**–**e**)

PZT transducer vibrates at a resonance frequency, the orifice plate generates a vibration mode that resembles the deformation mode in Fig. 2. When the applied voltage frequency is constant, the deformation shape does not change, and the orifice plate displacement is proportionate to the applied voltage. In this mode, the deformation of the center part is larger, and the particle near the center is excited with greater force. As the orifice plate's displacement increases, the orifices open from inside one by one (Fig. 2b–d). For proportional flow rate, the number of opened orifices should be proportionate to applied voltage. In this condition, the difference of the applied voltage from state of Fig. 2b, where the first orifice gets open, to state of Fig. 2c, where the second orifice gets open, should be the same as the difference of the applied voltage from state of Fig. 2c to state of Fig. 2d, where the third orifice gets open. That should apply to all orifice numbers and, making that voltage difference represented by $\Delta V$, we can approximate the effective cross sectional area. In this condition, the effective cross sectional area of the valve is the sum of sectional area of orifices. When an orifice sectional area is $s_{eo}$, the effective cross sectional area $S_e$ is represented by:

$$S_e = \frac{V - V_{\min}}{\Delta V} s_{eo} + s_{eo} \tag{4}$$

where $V$ is applied voltage and $V_{\min}$ is the voltage with which the first orifice gets open. So that Eq. (4) stands up, the $V_{min}$, $\Delta V$ and applied pressure should be constant and the voltage range should be between the voltage with which the first orifice opens and the voltage with which the last orifice opens. When the air pressure is large enough, the flow becomes choke condition and the flow rate $Q$ is decided by

$$Q = KS_eP\sqrt{\frac{273}{\theta}} \tag{5}$$

where $K$ is proportionality constant, $P$ is supplied air pressure and $\theta$ is temperature of the inner valve [33]. From Eqs. (4) and (5), flow rate is proportional to effective cross sectional area and consequently is proportionate to applied voltage. For a proportional flow rate change, the orifice position should be fitted to the orifice plate deformation shape.

## Prototype design

### Configuration of prototype

To design the orifice position, the orifice plate's vibration shape is needed. In this section, we explain the prototype condition. The prototype is designed to improve the previous model using a bolt-clamped Langevin type transducer (BLT) and Fig. 3 shows a cross section of the prototype whose mechanism can generate large acceleration at the orifice plate [30]. The prototype long is 80 mm and diameter of main part is 20 mm. This transducer, which generates longitudinal vibration, has two ring-type PZTs with the directional polarization of the thickness. The orifice plate, which forms the transducer's top, is the antinode of the vibration, and it vibrates at the BLT's resonance frequency. The BLT is designed so that the flange and PZT parts are at the vibration node. This transducer

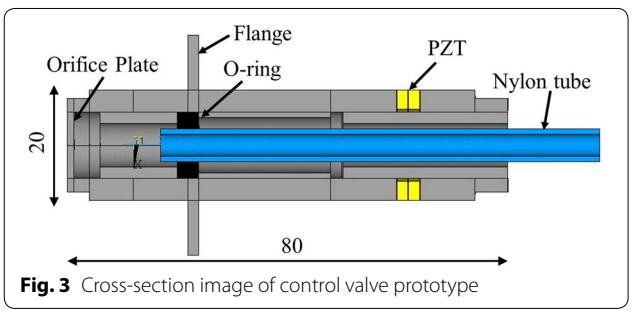


**Fig. 3** Cross-section image of control valve prototype

is hollow, and an air tube is attached to the inner flange by a rubber O-ring. Therefore, the space from the O-ring to the orifice plate becomes the air chamber. The orifice plate diameter is 12 mm and the thickness of orifice plate is 0.8 mm. Figure 4 shows the FEM results of the resonance condition. From this result, the orifice plate is the antinode and the orifice plate generates large vibration deformation. Figure 5 shows the components of the prototype, which consists of a main body and a bolt that attaches the orifice plate, the orifice plate, a bolt that attaches the PZTs, a nut, ring-type PZTs, and electrodes. The prototype is made of stainless steel, except the PZTs and electrodes. The orifice plate has 12 orifices whose diameter is 0.4 mm and orifice condition is shown at next section. The PZTs' outer diameters are 20 mm, inner diameters are 13 mm, and thicknesses are 4 mm. The electrodes are made of copper. The particles are 0.8 mm diameter stainless steel. Figure 6 shows the assembled prototype and its weight is 150 g.

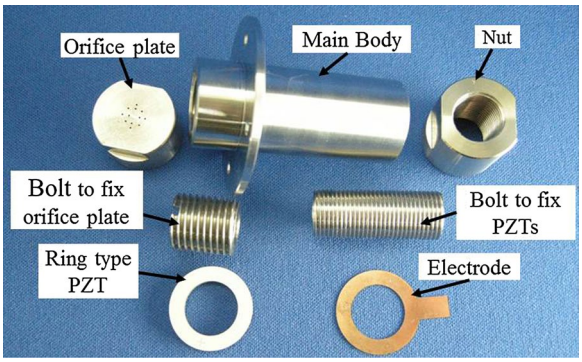


**Fig. 5** Components of prototype

### Orifice position design for proportional flow condition

In this section, we explain the method to design orifice position using shape of orifice plate deformation generated by vibration. We approximated the orifice plate's deformation shape, using a clamped circular plate deformation. The clamped plate's deformation is determined by the following equation:

$$u(r) = \frac{1}{D}\frac{P}{64}\left(a^2 - r^2\right)^2, \tag{6}$$

where $u$ is the plate's deformation, $P$ is the stress, $D$ is the flexural rigidity, $a$ is the plate's radius, and $r$ is the distance from its center [34]. The stress depends on the voltage applied to the transducer, and the flexural rigidity is constant. The center part of the deformation ($r = 0$) is:

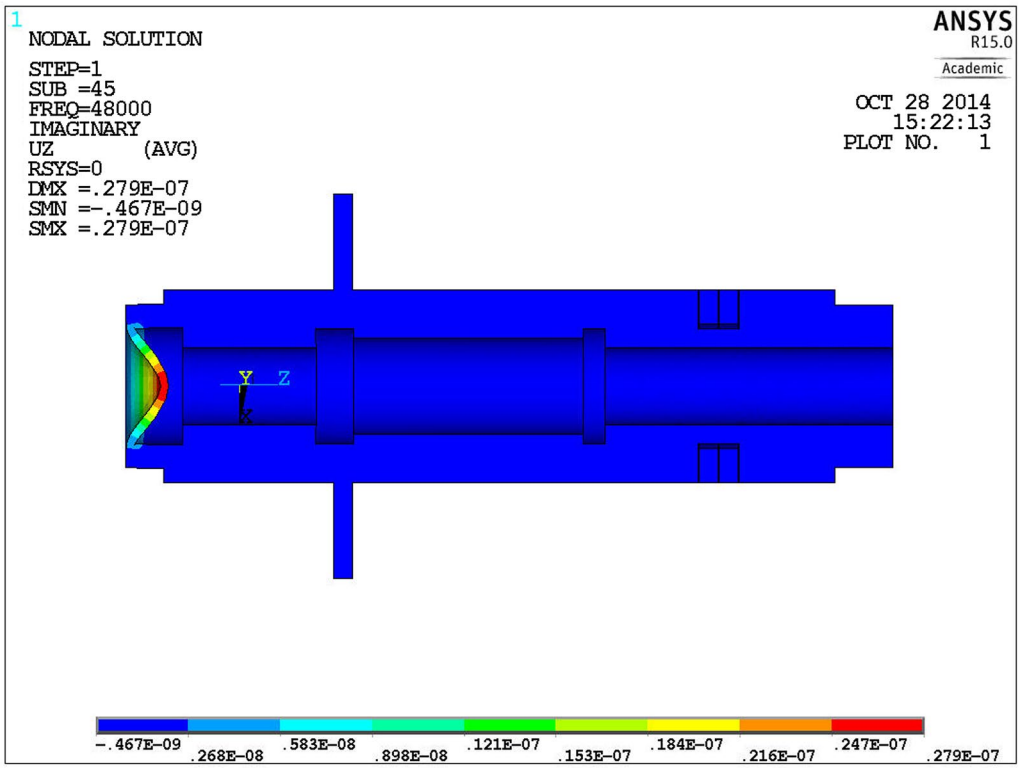


**Fig. 4** FEM result of deformation mode of the prototype

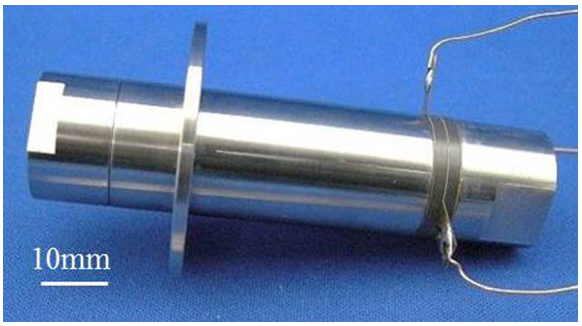


**Fig. 6** Assembled prototype

$$u(0) = \frac{Pa^4}{64D}. \tag{7}$$

For simplification, the relation is calculated between the distance from the center of the orifice plate and the reduction of the displacement ratio using Eqs. (6) and (7):

$$\omega(r) = \left(a^2 - r^2\right)^2 / a^4. \tag{8}$$

Deformation ratio $\omega(r)$ of the orifice plate depends on the distance from its center. When the orifice plate displacement is proportional to the applied voltage, voltage *V(r)*, which is needed to open the orifice at any distance from the center, is calculated:

$$V(r) = \frac{V_c}{\omega(r)}, \tag{9}$$

where $V_c$ is the voltage needed to open the orifice at the center and $r$ is the distance from its center. Using Eq. (9), to choose a proper orifice position, the minimum and maximum applied voltages as well as the orifice number are needed. The minimum and maximum applied voltages depend on respectively the innermost and outermost orifice positions. The following $V_{\min}$ voltage opens the innermost orifice, and $V_{\max}$ opens the outermost orifice.

$$V_{\min} = \frac{V_c}{\omega(r_{\min})} \tag{10}$$

$$V_{\max} = \frac{V_c}{\omega(r_{\max})}. \tag{11}$$

The voltage difference $\Delta V$ is decided by $V_{\max}$, $V_{\min}$ and the number of orifices. $\Delta V$ is determined by:

$$\Delta V = \frac{V_{\max} - V_{\min}}{N - 1}, \tag{12}$$

where $N$ is the total number of orifices and it is constant number.

Using Eq. (12), the Eq. (4) becomes simple:

$$S_e = (N-1)\left(\frac{V - V_{\min}}{V_{\max} - V_{\min}}\right)s_{eo} + s_{eo}. \tag{13}$$

When the applied pressure is constant and consequently $V_{min}$ and $V_{max}$ are constant, increase of effective cross sectional area changes in proportion to applied voltage, from first orifice opening to final orifice opening.

In this condition, $V_{\mathrm{n}}$, which is needed to open the $n$th orifice from the innermost orifice position, is expressed using $\Delta V$:

$$V_n = V_{\min} + (n-1)\Delta V. \tag{14}$$

On the other hand, $V_{\mathrm{n}}$ and $r_{\mathrm{n}}$ were calculated for the $n$th orifice relations using Eq. (8):

$$V_n = \frac{V_c}{\omega(r_n)}. \tag{15}$$

Inserting Eq. (14) into Eq. (15) yields the following equation:

$$V_{\min} + (n-1)\Delta V = \frac{V_c}{\omega(r_n)}. \tag{16}$$

Inserting Eqs. (10), (11), and (12) into Eq. (16) yields:

$$\frac{1}{\omega(r_n)} = \frac{1}{\omega(r_{\min})} + \left(\frac{n-1}{N-1}\right)\left(\frac{1}{\omega(r_{\max})} - \frac{1}{\omega(r_{\min})}\right). \tag{17}$$

From these results, the orifice plate's condition is determined by the innermost and the outermost orifice positions and the orifice numbers. Even though the $V_{min}$ and $V_{max}$ are changed by supplied air pressure, the condition is kept where the flow rate is proportional to the applied voltage because the change rate of $V_{min}$ and $V_{max}$ are same.

Using Eq. (8), orifice position $r_{\mathrm{n}}$ is decided by $\omega(r_n)$.

$$r_n = \sqrt{a^2 - a^2\sqrt{\omega(r_n)}}. \tag{18}$$

The orifice position is determined by the innermost and the outermost orifice positions and the orifice numbers, and the valve's sectional area changes in proportion to the applied voltage.

To select the orifice position, we need the orifice plate's displacement ratio at each location. The FEM results and the calculated result determine the orifice position. Figure 7 shows the relationship between the orifice plate's displacement ratio and the distance from its center. The continuous line indicates FEM results, and the dashed line represents the results calculated by Eq. (8). The orifice plate has 6 mm radius and $a = 6$ means orifice plate edge. As shown in Fig. 7, the results

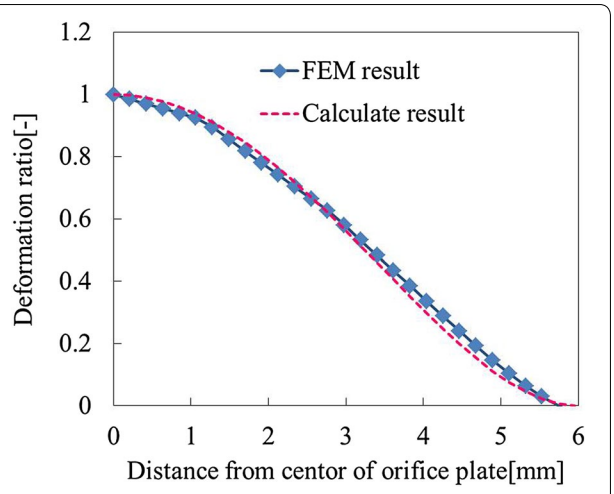


**Fig. 7** Comparison of calculated and FEM results of deformation ratio

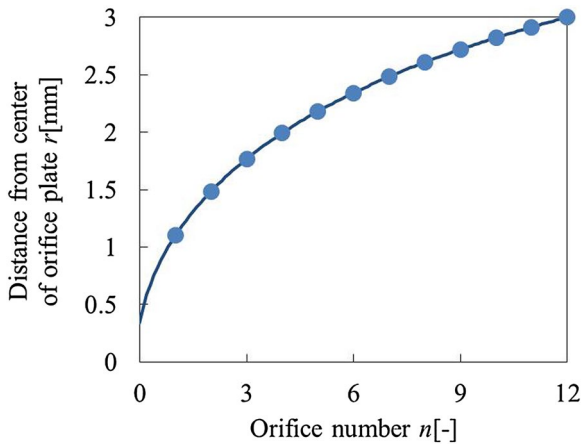


**Fig. 8** Relationship between orifice number and distance from center of orifice plate

are close and the orifice position can be designed. Because the calculated and FEM results are close inside the 3.0-mm radius, the outermost position is decided at 3.0 mm. In this report, the diameter of particles is 0.8 mm and the innermost orifice position is decided at 1.1 mm to avoid the crash of each particle. From Fig. 7, the displacement ratio is 95% at 1.1 mm and 60% at 3.0 mm. The orifices are located at equal distance from each other as possible. In this study, the total number of orifices is 12, and their diameter is 0.4 mm. Under 0.6 MPa, the maximum flow rate is about 80 L/min, and the minimum flow rate is about 7 L/min. In this condition, outermost orifice position is 3.0 mm and innermost orifice position is 1.1 mm and $\omega(r_{max})$ and $\omega(r_{min})$ are decided by Eq. (8). $\omega(r_{min})$ is 0.934 and $\omega(r_{max})$ is 0.563. When $N$ is 12, $\omega(r_n)$ is decided integrating these values into Eq. (17).

$$\omega(r_n) = \frac{11}{11.78 - 0.706(n-1)} \tag{19}$$

From this equation, $\omega(r_n)$ is decided by orifice number $n$. The distance from center of orifice plate is calculated using Eqs. (18) and (19). Figure 8 shows the relationship between orifice number and distance from center of orifice plate. The orifices are numbered from inner to outer. Table 1 shows the orifice position in designed orifice plate. Figure 9a shows the orifice position and Fig. 9b shows photograph of orifice part.

## Basic characteristics of the prototype

Next we checked the basic characteristics of the designed prototype: the resonance frequency and the vibration condition. We checked the prototype's resonance frequency using frequency response analyzer and measured the vibration acceleration with a laser vibrometer. Figure 10 shows the relationship between the frequency of the applied voltage and the admittance when the applied voltage is 2 $V_{p\text{-}p}$. From this result, the admittance and phase changed notably at 47 kHz. The valve's resonance frequency was about 47 kHz. Figure 11 shows the relationship between the frequency of the applied voltage and the center's acceleration. When the applied voltage was 20 $V_{p\text{-}p}$, the transducer achieved maximum vibration acceleration at 47.13 kHz, and when the applied voltage was 120 $V_{p\text{-}p}$, it achieved maximum vibration acceleration at 46.95 kHz. These results show that the transducer vibration frequency was changed by the applied voltage. To reduce influence of the vibration frequency change by applied voltage, driving frequency was determined

**Table 1 Relationship between orifice number and distance from center of orifice plate**

| Orifice number $n$ (—) | Distance from center of orifice plate $r$ (mm) |
|---|---|
| 1 | 1.10 |
| 2 | 1.46 |
| 3 | 1.75 |
| 4 | 1.98 |
| 5 | 2.17 |
| 6 | 2.34 |
| 7 | 2.48 |
| 8 | 2.60 |
| 9 | 2.72 |
| 10 | 2.82 |
| 11 | 2.91 |
| 12 | 3.00 |

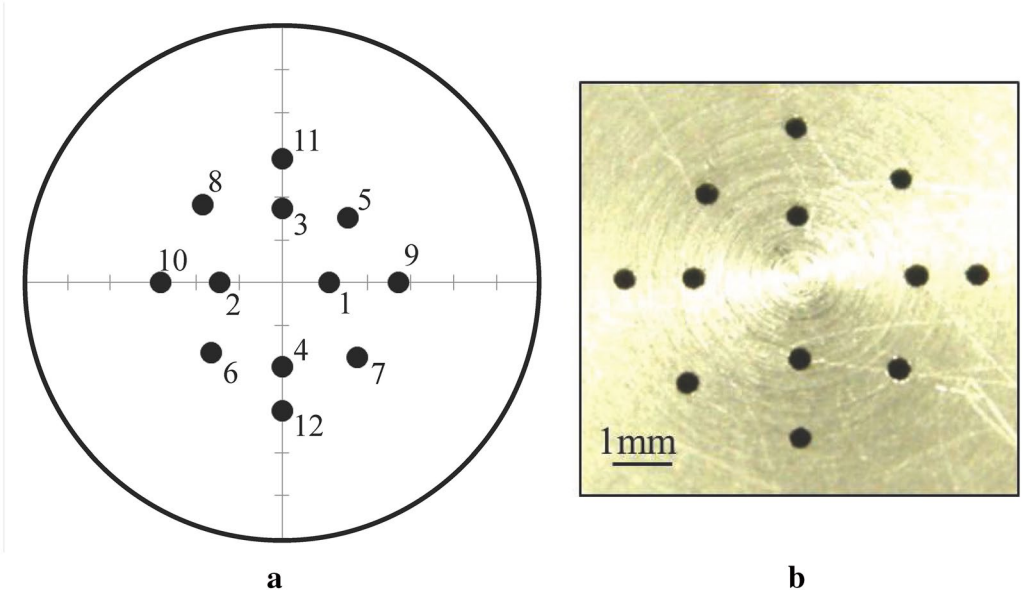


**Fig. 9** Orifice positions (**a**, **b**)

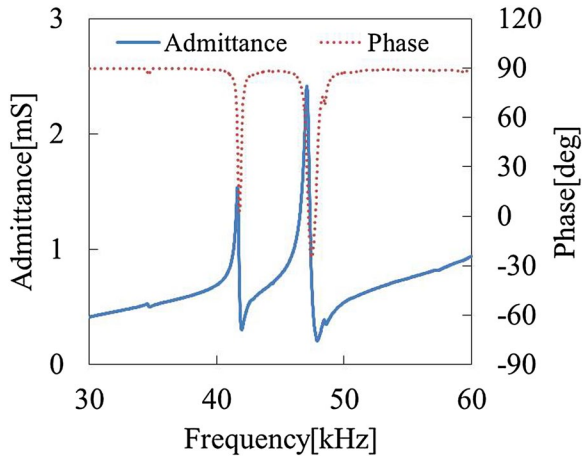


**Fig. 10** Relationship between admittance of the prototype, phase and frequency

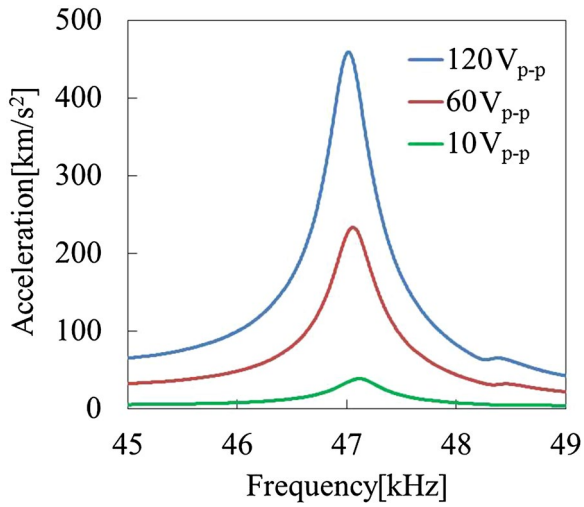


**Fig. 11** Relationship between prototype's acceleration and frequency

experimentally. Figure 12 shows relationship between applied voltage and vibration acceleration of orifice plate when the driving frequency is 46.10 kHz. From Fig. 12, the acceleration of orifice plate is proportional to applied voltage, under both increasing and decreasing applied voltage. From this result, this driving frequency is suitable for flow control experiment. Next, we checked vibration-mode shape using laser Doppler velocimetry and compared it with the analytical results (Fig. 13). Since the orifice plate deformation ratio is near the suppositional mode, the orifices are at the optimal position.

## Flow rate characteristics

Finally, we investigated the flow rate characteristics. Figure 14 shows the experimental setup used to measure them. This system consists of a function generator, a voltage amplifier, a compressor, an air tank, an air pressure gauge, and a flow meter. When the control valve is driven, the air flow is ejected. We measured the relation between the voltage applied to the PZT and the change in the flow rate. The flow meter is a thermal-type (CKD FSM2-101).

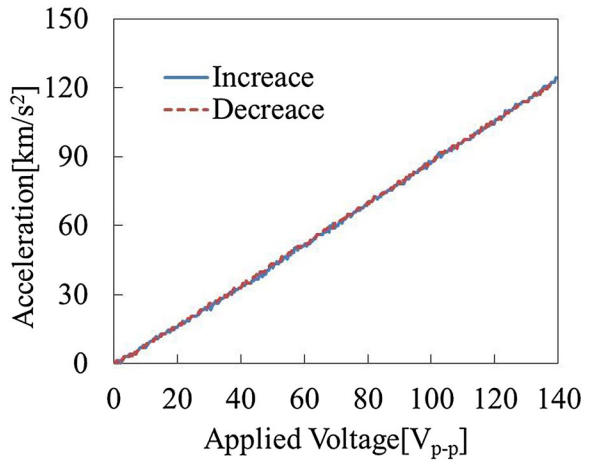


**Fig. 12** Relationship between applied voltage and prototype's acceleration

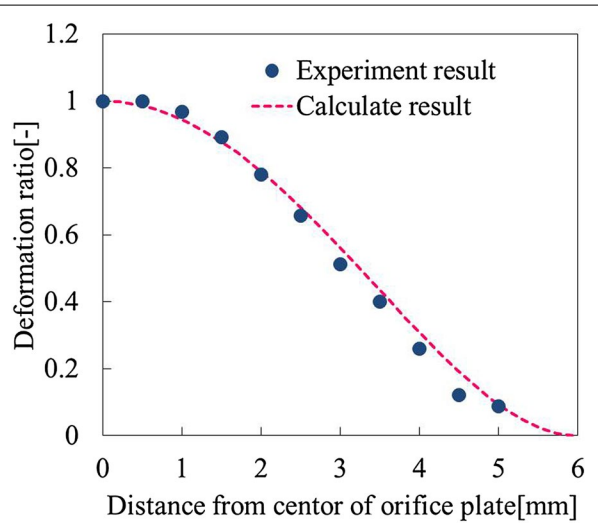


**Fig. 13** Comparison of calculated result and actual deformation ratio value

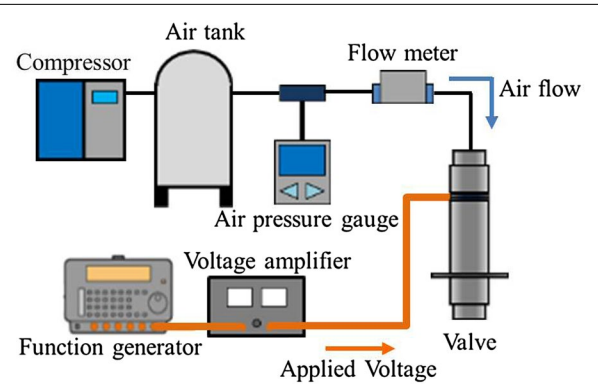


**Fig. 14** Experimental setup for flow control

In this mechanism, we cannot check the number of particle on orifice plate. For stable condition, we used a larger number of particles than the number of orifices, encapsulating 30 particles. We also conducted experiments by supplying pneumatic pressure of 0.4–0.6 MPa in 0.1-MPa increments. The applied voltage varied from 0 to 140 $V_{p\text{-}p}$ and, to check the static condition, the varied time was decided on 240 s. Additionally, the orifice plate center's acceleration was checked by a laser vibrometer and a lock-in amplifier. The experimental results are shown in Fig. 15.

From Fig. 15, the flow control valve smoothly changed the airflow except at low flow rate. The acceleration state under low applied voltage was different from that of Fig. 12. However, when the applied voltage was high enough and the flow rate sure changed, the acceleration was proportional to the applied voltage and was not influenced by the flow rate nor the air pressure conditions. The flow conditions changed between low flow rate and high flow rate. This phenomenon occurred in all of the pressure conditions. We checked the relationship between the flow rate condition and the orifice acceleration. Figure 16 shows the flow rate condition, the innermost orifice acceleration, and the outermost orifice acceleration on 0.4 MPa. Both accelerations were calculated by the center's acceleration and the value in Fig. 11. From Fig. 16, the flow rate achieved maximum value at about 92 $V_{p\text{-}p}$. In this condition, the outermost orifice acceleration achieved a value of 46.5 km/s$^2$ and outermost orifice opened. The innermost orifice acceleration is 46.5 km/s$^2$ at about 58 $V_{p\text{-}p}$, and the flow rate condition is changed at this voltage. From this result, the innermost orifice gets open when the applied voltage is 58 $V_{p\text{-}p}$ at 0.4 MPa. The particle movements are imagined by experimental results. Figure 17 shows an image of particle motion. When the acceleration value is small, the particle doesn't move with the orifice plate (Fig. 17a). Figure 17b shows the particle movement state. When the acceleration increases, the particle starts moving and generates a gap between the orifice and the particle that changes with the acceleration and an increasing flow rate. Figure 17c shows the orifice opening state. In this condition, the particle is moved away from the orifice by the vibration and the orifice maintains the opening condition except the moving particles irregularly close. Because this state's condition conforms to that required in the designed state, the flow rate is proportionate to the applied voltage when the voltage is between 58 and 92 $V_{p\text{-}p}$. This phenomenon occurred in all the pressure conditions. Therefore, the flow rate is proportionate to the applied voltage regardless of the pressure scale except under a low flow rate. On the other hand, the flow rate characteristics have temporal increase and decrease. This

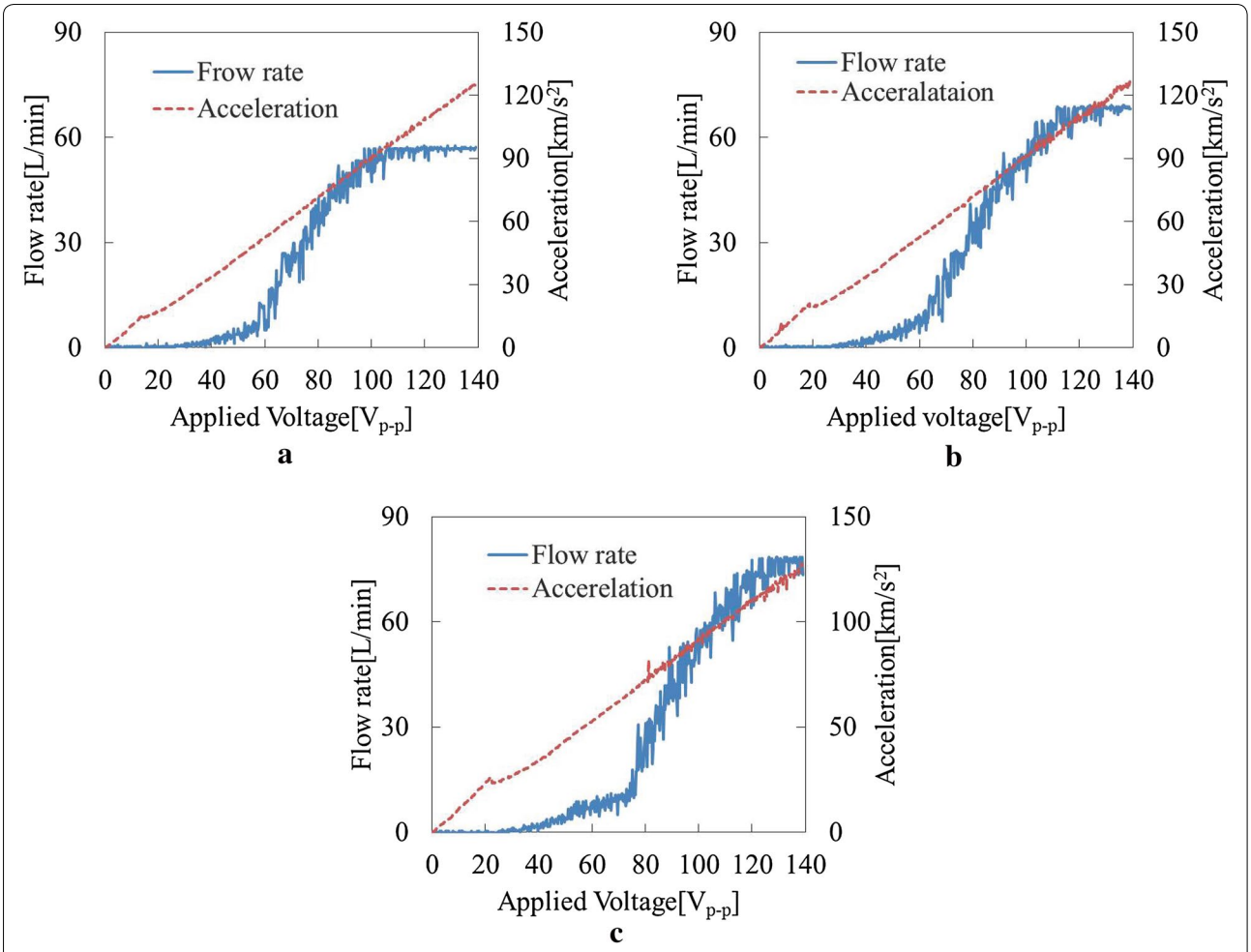


**Fig. 15** Relationship between flow rate, acceleration and applied voltage **a** 0.4 MPa, **b** 0.5 MPa, **c** 0.6 MPa

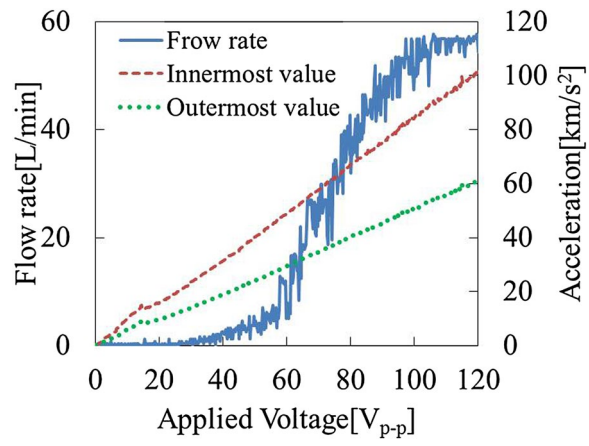


**Fig. 16** Relationship between flow rate and acceleration

was because the particles opened and closed irregularly. When the flow rate increases, the number of moving particles increases, and the flow rate varies temporally. Optimizing the orifice size, the number of orifices and the particle size could solve this problem.

Finally, we established the hysteresis characteristics and measured the flow rate change when the applied voltage increased and decreased with low speed. The applied voltage changed from 0 to 140 $V_{p\text{-}p}$ and 140 to 0 $V_{p\text{-}p}$. Figure 18 shows the experimental results at 0.5 MPa. The applied voltage changed from 0 to 140 $V_{p\text{-}p}$ and 140 to 0 $V_{p\text{-}p}$ with 240 s. In this control valve, the particles close orifices perfectly when flow rate decrease, and increase in flow rate and decrease in flow rate are close value. From this result, the valve is low hysteresis when applied voltage changes slowly.

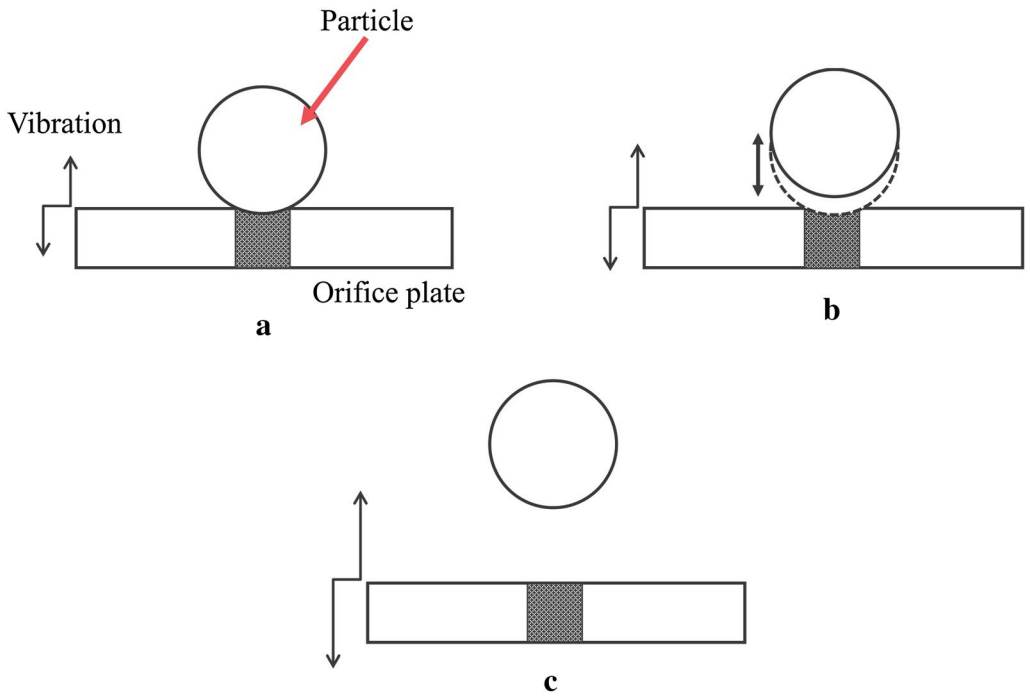


**Fig. 17** Image of particle movement (**a**–**c**)

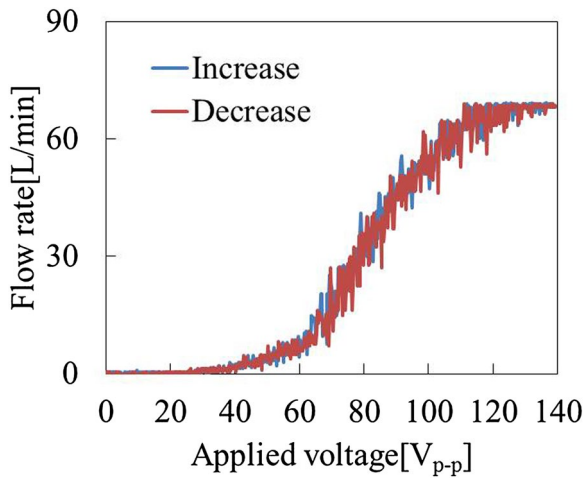


**Fig. 18** Hysteresis of flow control valve

## Conclusion

We explained how to control proportionally the airflow using a particle-excitation valve. This method required the orifice plate deformation shape and the orifice position. In this paper, we designed the experimental prototype using a bolt-clamped Langevin type transducer that can generate the large vibration acceleration at orifice plate. And we designed the orifice position using approximated orifice plate deformation. Next, we also analyzed prototype's basic characteristics and decided the driving condition. Finally, the prototype's flow rate control characteristics were evaluated. This control valve can proportionally control the airflow when the acceleration is proportional to the applied voltage and orifice acceleration exceeds the orifice opening condition. These characteristics were stably generated under changing air pressures: 0.4, 0.5, and 0.6 MPa. Additionally, the prototype shows stable flow characteristics when flow rate decreases. We conclude that this mechanism has potential to create proportional valves with many advantages.

#### Authors' contributions

DH carried out the main part of the studies and drafted the manuscript. TY and NF joined discussion and evaluated experimental results. KS and TK participated in design of the prototype and experimental method. All authors read and approved the final manuscript.

#### Author details

[1] Department of Mechanical Engineering, Kansai University, 3-3-35, Yamate-cho, Suita-shi, Osaka 564-8680, Japan. [2] Graduate School of Engineering, Tokyo Institute of Technology, 2-12-1 Ookayama, Meguro-ku, Tokyo 152-8550, Japan. [3] Graduate School of National Science and Technology, Okayama University, 3-1-1 Tsushima-naka, Okayama 700-8530, Japan.

#### Acknowledgements

This work was supported by JSPS KAKENHI Grant Number 15K21519.

#### Competing interests

The authors declare that they have no competing interests.

#### Availability of data and materials

Not applicable.

**Consent for publication**
Not applicable.

**Ethics approval and consent to participate**
Not applicable.

**Funding**
Not applicable.

## Publisher's Note



Received: 25 May 2017 Accepted: 3 October 2017
Published online: 11 October 2017

**References**

1. Hong YP, Koo D, Park J, Kim S, Kim KS (2015) The Softgait: a simple and powerful weight-support device for walking and squatting. In: 2015 IEEE/RSJ international conference on intelligent robots and systems, pp 6338–6341
2. Hashimoto Y, Nagase J, Saga N, Satoh T (2016) Development and control of support function for upper limb support device. In: 2016 IEEE international conference on industrial technology, pp 1566–1571
3. Nomura K, Yonezawa T, Ogitsu T, Mizoguchi H, Takemura H (2015) Development of stewart platform type ankle-foot device for trip prevention support. In: 2015 37th annual international conference of the IEEE engineering in medicine and biology society, pp 4808–4811
4. Sanada K, Akiyama Y (2011) Power-assist chair using pneumatic actuator. Int J Autom Technol 5(4):502–507
5. Yagi E, Harada D, Kobayashi M (2009) Upper-limb power-assist control for agriculture load lifting. Int J Autom Technol 3(6):716–722
6. Li X, Noritsugu T, Takaiwa V, Sasaki D (2013) Design of wearable power assist wear for low back support using pneumatic actuators. Int J Autom Technol 7(2):228–236
7. Ribuan MN, Wakimoto S, Suzumori K, Kanda T (2016) Omnidirectional soft robot platform with flexible actuators for medical assistive device. IJAT 10(4):497–501
8. Akagi T, Dohta S, Matsui Y, Tamaki H, Kato N (2016) Low-cost wearable rehabilitation devices using flexible pneumatic cylinder with built-in pneumatic driving system. In: 2016 IEEE international conference on advanced intelligent mechatronics (AIM), pp 89–93
9. Loh CT, Tsukagoshi H (2014) Pneumatic big-hand gripper with slip-in tip aimed for the transfer support of the human body. In: 2014 IEEE international conference on robotics & automation, pp 475–481
10. Kurumaya S, Suzumori K, Nabae H, Wakimoto S (2016) Musculoskeletal lower-limb robot driven by multifilament muscles. Robomech J 3:18
11. Ueda H, Akagi T, Dohta S (2010) Development of 2-position 3-port control valve with self-holding function. In: Proceedings of SICE annual conference 2010, pp 1239–1243
12. Nasir A, Akagi T, Dohta S, Ono A (2015) Analysis of low-cost wearable servo valve using buckled tubes for optimal arrangement of tubes. In: 2015 IEEE international conference on advanced intelligent mechatronics, pp 831–835
13. Li B, Gao L, Yang G (2013) Evaluation and compensation of steady gas flow force on the high-pressure electro-pneumatic servo valve direct-driven by voice coil motor. Energy Convers Manag 67:92–102
14. Jien S, Hirai S, Honda K (2010) Miniaturization design of piezoelectric vibration-driven pneumatic unconstrained valves. JRM 22(1):91–99
15. Fritz KP, Mayer V, Steffens T, Kück H (2010) Switching valve with isolated impact actuator. In: 12th International conference on new actuators, pp 242–245
16. Yun SN, Ham YB, Park JH, So HJ, Lee IY (2008) Pneumatic valve with a pressure regulator for bimorph type PZT actuator. J Electroceramics 20:215–220
17. Yun SN, Jeong HH, Kim DG, Jeong EA, Kim HH (2011) New strategy for design and fabricating of a grain sorting system using high-speed piezoelectric valves. In: Proceedings of the 8th JFPS international symposium on fluid power, OKINAWA 2011, 1D-1, pp 270–275
18. Zeng H, Yuan RB, Sun C, Zhang Z (2012) Study on performance of laminated piezoelectric pneumatic servo valve. Proc Eng 31:1140–1148
19. Park JH, Yoshida K, Yokota S (1999) Resonantly driven piezoelectric micropump fabrication of a micropump having high power density. Mechatronics 9:687–702
20. Gang B, Tinghai C, Yao H, Xiangdong G, Han G (2011) A nozzle flapper electro-pneumatic proportional pressure valve driven by piezoelectric motor. In: Proceedings of 2011 international conference on fluid power and mechatronics, pp 191–195
21. Lingcong N, Xiaoxian Y, Qing L (2008) Modeling and simulation of ultrasonic motor driving jet-pipe servo valve system. In: 2008 Asia simulation conference-7th international conference on system simulation and scientific computing, pp 689–692
22. Bang YB, Joo CS, Lee KL, Hur JW, Lim WK (2003) Development of a two-stage high, speed electrohydraulic servo valve system using stack-type piezoelectric-elements. In: Proceedings of the 2003 IEEE/ASME international conference on advanced intelligent mechatronics, pp 131–136
23. Karunanidhi S, Singaperumal M (2010) Design, analysis and simulation of magnetostrictive actuator and its application to high dynamic servo valve. Sens Actuators A 157:185–197
24. Sente P, Vloebergh C, Labrique F, Alexandre P (2008) Control of a direct-drive servo-valve actuated by a linear amplified piezoelectric. In: Proceedings of the 2008 international conference on electrical machines, 1051, pp 1–6
25. Zhang D, Lv J, Jiang Y, Chen H, Fu J (2014) A piezoelectric microvalve with a flexure-hinged driving frame and microfabricated silicon sealing pair. Mechatronics 24:511–518
26. Jeon J, Nguyen QH, Han YM, Choi SB (2013) Design and evaluation of a direct drive valve actuated by piezostack actuator. Adv Mech Eng 986812:1–12
27. Lindler JE, Anderson EH (2002) Piezoelectric direct drive servovalve. In: Industrial and commercial applications of smart structures technologies 2002, 4698-53, pp 1–9
28. Zhou M, Gao W, Yang Z, Tian Y (2012) High precise fuzzy control for piezoelectric direct drive electro-hydraulic servo valve. J Adv Mech Des Syst Manuf 6(7):1154–1167
29. Hirooka D, Suzumori K, Kanda T (2009) Flow control valve for pneumatic actuators using particle excitation by PZT vibrator. Sens Actuators A 155(2):285–289
30. Hirooka D, Yamaguchi T, Furushiro N, Suzumori K, Kanda T (2016) Development of novel particle excitation flow control valve for stable flow characteristics. Int J Autom Technol 10(4):540–548
31. Hirooka D, Suzumori K, Kanda T (2011) Design and evaluation of orifice arrangement for particle-excitation flow control valve. Sens Actuators A 171(2):283–291
32. Hirooka D, Yamaguchi T, Furushiro N, Suzumori K, Kanda T (2017) Particle-excitation flow control valve using piezo vibration-improvement for high flow rate and research on controllability. IEEJ Trans Sens Micromach 137(1):32–37
33. Kawashima K, Kagawa T, Fujita T (2000) Instantaneous flow rate measurement of ideal gases. J Dyn Syst Meas Control 122:174–178
34. Timoshenko S, Krieger SW (1959) Theory of plates and shells, 2nd edn. McGraw-Hill, New York